Arch. Mech., **65**, 5, pp. 407–428, Warszawa 2013

Gradient-enhanced damage model for large deformations of elastic-plastic materials

B. WCISŁO[1)], J. PAMIN[1)], K. KOWALCZYK-GAJEWSKA[2)]

[1)] *Institute for Computational Civil Engineering*
Cracow University of Technology
Warszawska 24
31-155 Kraków, Poland
e-mails: bwcislo@L5.pk.edu.pl, jpamin@L5.pk.edu.pl

[2)] *Institute of Fundamental Technological Research*
Polish Academy of Sciences
Pawińskiego 5B
02-106 Warszawa, Poland
e-mail: kkowalcz@ippt.pan.pl

This paper deals with the development of a family of gradient-enhanced elasticity-damage-plasticity models for the simulation of failure in metallic and composite materials. The model incorporates finite deformations and is developed with the assumption of isotropy and isothermal conditions. The gradient enhancement applied to the damage part of the model aims at removing pathological sensitivity to the finite element discretization which can occur due to material softening.
The attention is focused on the algorithmic aspects and on the implementation of the model using AceGen tool. The numerical verification tests of the described model are performed using the Mathematica-based package AceFEM. Particularly, uniaxial tension test for a bar with a variable cross-section and tension of a perforated plate are examined.

Key words: large strains, damage, plasticity, gradient-enhancement, AceGen package.

1. Introduction

The research presented in this paper is focused on the development of a family of gradient-enhanced elasticity-plasticity-damage models in large strain regime. The models can be used to reproduce the behaviour of metals and composites, however, are not directly focused on a specific material.

A material model including damage can involve a descending stress-strain branch (the post-peak regime). This situation can cause ill-posedness of the boundary value problem which results in a pathological mesh-sensitivity in the

numerical simulations. To obtain a material model which is able to reproduce damage properly a regularization should be applied, for instance nonlocal models or higher-order gradient theories. Alternatively, discontinuous modelling using cohesive elements, e.g. [1], can be employed. The implicit gradient averaging which is used in the presented model was firstly adopted by Peerlings *et al.* [2]. The majority of publications concerning gradient averaging for damage-plastic models is restricted to the assumption of small strains. The finite strain formulations are presented in publications of Steinmann [3] (hyperelastic-damage continuum), Geers [4] (plasticity with softening) and Areias [5] (plasticity coupled with damage). When applying the gradient regularization to the geometrically non-linear models one has to make a decision which configuration should be chosen to perform averaging. What is more important, by accounting for large strains the problem becomes more difficult due to softening caused by the geometrical effects such as necking.

In the paper the attention is focused on the implementation aspects of the presented model within the Mathematica-based packages AceGen/AceFEM created by Korelc [6]. Due to the novel symbolic-numerical approach to the finite element computations the particular solution algorithm taking the advantage of automatic differentiation is applied. Moreover, the algorithm is flexible and different material laws, for instance different yield criteria, can easily be applied. The constitutive model presented in the second section is based mainly on the concepts presented in [7], [5] and [8]. After the discussion of the implementation and the solution algorithm the selected results of the numerical simulations performed with AceFEM are presented. Particularly, the influence of the applied finite element type on the obtained results, as well as the effects of choice of configuration for averaging and of the strain measure governing damage are investigated. Finally, some conclusions and suggestions for future work are gathered.

2. Constitutive relations

The kinematical framework of the material model is based on a classical multiplicative decomposition of the deformation gradient into its elastic and plastic components [9]

$$\mathbf{F} = \mathbf{F}^e \mathbf{F}^p. \tag{2.1}$$

The main internal variable is assumed to be elastic left Cauchy–Green tensor

$$\mathbf{b}^e = \mathbf{F}^e \mathbf{F}^{eT}. \tag{2.2}$$

The free energy function is assumed as an isotropic function of the elastic left Cauchy–Green tensor $\mathbf{b}^e$, a scalar measure of accumulated plastic flow γ and

a scalar damage parameter ω

$$\psi = (1-\omega)\psi^e(\mathbf{b}^e) + \psi^p(\gamma). \tag{2.3}$$

The relationship between the Kirchhoff stress tensor and elastic left Cauchy–Green tensor is expressed through the elastic part of free energy function and it takes the form

$$\boldsymbol{\tau} = 2\frac{\partial \psi^e}{\partial \mathbf{b}^e}\mathbf{b}^e. \tag{2.4}$$

The Kirchhoff stress tensor can be decomposed into its deviatoric and volumetric parts:

$$\boldsymbol{\tau} = p\boldsymbol{I} + \boldsymbol{t}, \qquad p = (\boldsymbol{\tau} : \boldsymbol{I})/3, \qquad \boldsymbol{t} = \boldsymbol{\tau} - p\boldsymbol{I}. \tag{2.5}$$

In the constitutive description damage is understood as the degradation of the elastic free energy function with scalar damage variable ω

$$\psi^{e,d} = (1-\omega)\psi^e. \tag{2.6}$$

The scalar damage parameter ω grows from zero for the intact material to one for a complete material destruction. The damage evolution law which determines the value of ω is a function of a history parameter κ

$$\omega = f^d(\kappa) \tag{2.7}$$

and can be formulated in different ways depending on the considered material, see, e.g., [4]. The parameter κ in Eq. (2.7) is obtained through the formula

$$\kappa = \max(\tilde{\epsilon}, \kappa_0), \tag{2.8}$$

where κ_0 describes the damage threshold and $\tilde{\epsilon}$ is an equivalent local strain or energy measure.

The choice of the damage governing quantity $\tilde{\epsilon}$ which should be applied in the model including large strains will be discussed now. In the literature different measures can be encountered, for instance stored energy [3] or accumulated plastic strain [5], [8]. In the paper we assume that the damage process is not directly determined by the plastic flow but it is governed by a total deformation measure. In particular, two measures are taken into account:

$$\tilde{\epsilon} = \det(\boldsymbol{F}) - 1, \tag{2.9}$$

$$\tilde{\epsilon} = \sqrt{(e_1^+)^2 + (e_2^+)^2 + (e_3^+)^2}, \tag{2.10}$$

where e_i^+ is a positive value of i-th eigenvalue of the Almansi strain tensor. The first measure (2.9) is closely connected with the increase of the material volume and can be related to the growth of the voids and cracks in the damage process. According to this model damage will not occur for the incompressible materials or for deformation involving volume reduction.

The second measure (2.10) is related to principal stretches by taking into account the positive eigenvalues of Almansi strain tensor. Consequently, in the second case incompressible materials can exhibit damage since also in a compression test the local measure can grow, however in a different way than for tension. For a tensioned sample damage is governed by a longitudinal strain whereas for compression by a transverse one. Thus, the choice of the proper deformation measure should be connected with the physical behaviour of material, observed in experiments.

The damage loading condition complemented with the set of Kuhn–Tucker conditions reads:

$$F_d(\tilde{\epsilon}, \kappa) = \tilde{\epsilon} - \kappa \leq 0, \qquad \dot{\kappa} \geq 0, \qquad \dot{\kappa} F_d(\tilde{\epsilon}, \kappa) = 0. \tag{2.11}$$

The plastic process is assumed to take place in the effective stress space, i.e., it governs the behaviour of the undamaged skeleton of the material. This approach is based on a principle of strain equivalence [10] which states that the damaged material responds to a given stress $\boldsymbol{\tau}$ in the same way as the undamaged material responds to the effective stress $\hat{\boldsymbol{\tau}}$

$$\hat{\boldsymbol{\tau}} = \frac{\boldsymbol{\tau}}{1-\omega}. \tag{2.12}$$

The plastic regime is defined through the yield function F_p which is an isotropic function of the effective Kirchhoff stress tensor $\hat{\boldsymbol{\tau}}$ and the measure of accumulated plastic flow γ

$$F_p(\hat{\boldsymbol{\tau}}, \gamma) = f(\hat{\boldsymbol{\tau}}) - \sqrt{\frac{2}{3}}(\sigma_{y0} - q(\gamma)) \leq 0. \tag{2.13}$$

The function $f(\hat{\boldsymbol{\tau}})$ represents selected plasticity function which in this work is assumed to be the Burzyński–Drucker–Prager (BDP) or the Huber–Mises–Hencky (HMH) criterion. The general formulation for the function f is written in the form

$$f = \sqrt{2J_2} + \frac{\alpha_p}{3} I_1, \tag{2.14}$$

where α_p is a material constant, I_1 and J_2 are invariants of the effective Kirchhoff stress tensor $\hat{\boldsymbol{\tau}}$ and its deviatoric part $\hat{\boldsymbol{t}}$:

$$I_1 = \hat{\boldsymbol{\tau}} : \boldsymbol{I}, \qquad J_2 = \frac{1}{2}\hat{\boldsymbol{t}}^2 : \boldsymbol{I}. \tag{2.15}$$

In the following numerical simulations, instead of the material constants α_p and σ_{y0} the initial yield threshold for tension σ_{t0} and compression σ_{c0} are given. The relations between these constants are expressed as [7]

$$\sigma_{y0} = 2\sqrt{\frac{2}{3}}\frac{\sigma_{c0}\sigma_{t0}}{\sigma_{c0}+\sigma_{t0}}, \qquad \alpha_p = 3\sqrt{\frac{2}{3}}\frac{\sigma_{c0}-\sigma_{t0}}{\sigma_{c0}+\sigma_{t0}}. \tag{2.16}$$

The function $q(\gamma)$ can be derived from the plastic part of the free energy

$$q(\gamma) = -\frac{d\psi^p(\gamma)}{d\gamma} \tag{2.17}$$

and represents the yield strength evolution, for instance isotropic linear hardening: $q(\gamma) = -h\gamma$.

The associative flow rule is assumed in the form [7]

$$-\frac{1}{2}\mathcal{L}_v\mathbf{b}^e = \dot{\gamma}\mathbf{N}\mathbf{b}^e, \tag{2.18}$$

where $\mathcal{L}_v$ is the Lie derivative of $\mathbf{b}^e$ and $\mathbf{N}$ is a normal to the yield function and $\dot{\gamma}$ is the plastic multiplier

$$\mathcal{L}_v\mathbf{b}^e = \mathbf{F}\frac{\partial}{\partial t}[(\mathbf{C}^p)^{-1}]\mathbf{F}^{\mathbf{T}}, \qquad \mathbf{N} = \frac{\partial F_p}{\partial \hat{\boldsymbol{\tau}}}. \tag{2.19}$$

3. Gradient enhancement

The incorporation of damage in the material description results in the decreasing stress-strain diagram which can cause the loss of ellipticity and ill-posedness of the boundary value problem. This situation manifests itself in the pathological mesh-sensitivity as the damage zone is localized in the smallest possible volume determined by the finite element discretization, for instance in one row of elements. To prevent the numerical solution from the mesh-sensitivity a regularization strategy is required. In the work an implicit gradient enhancement is applied [2]. The approach is motivated by micro-defect interactions and is numerically convenient.

In the gradient-enhanced damage model the local variable $\tilde{\epsilon}$ is substituted in damage condition (2.11a) with its non-local counterpart $\bar{\epsilon}$. The non-local variable is specified by the averaging equation

$$\bar{\epsilon} - l^2\nabla^2\bar{\epsilon} = \tilde{\epsilon} \tag{3.1}$$

with homogeneous natural boundary conditions [11]. The parameter l appearing in Eq. (3.1) is a material-dependent length parameter commonly called the internal length scale.

The application of gradient enhancement to the material model including large strains requires a decision which configuration is selected for averaging. If the Lagrangian (material) averaging is applied, the derivatives of the strain measure 3.1 are calculated with respect to the Lagrangian coordinates and the internal length is defined in the undeformed configuration. Consequently, during whole deformation process, the quantities for averaging are taken from the same material domain.

On the other hand, if Eulerian (spatial) averaging is considered then the internal length and the gradients in Eq. (3.1) are referred to the deformed configuration.

4. Implementation

The implementation of the model described above is performed using Mathematica-based packages AceGen and AceFEM developed by Korelc [6]. The former is a code generator which is capable of automatic differentiation and simultaneous optimization of expressions. The latter is a finite element environment which perfectly cooperates with AceGen, however, it can be replaced by other program like Abaqus or FEAP.

The AceGen package is used to create a code in a special meta-language for the calculation of contributions to the residual vector and the tangent matrix at each integration point of the element. Due to automatic differentiation the consistent tangent matrix is computed automatically and for that reason the consistent linearization of constutive equations is not considered in the paper.

To create a computationally efficient code with AceGen a particular approach, different than classical, should be applied. In simple terms, the residual vector $\mathbf{R}_u$ related to the virtual work formulation is computed as a derivative of the free energy function with respect to the vector of unknown displacements. If the relations between the approximated nodal displacements and the free energy function are specified properly, all differentiations and calculation of the final value of $\mathbf{R}_u$ are performed automatically. Similarly, the tangent stiffness matrix is calculated as a derivative of the residual vector $\mathbf{R}_u$ with respect to the vector of unknowns. The detailed explanation of the approach is included in [12] and [6].

The implementation of the described coupled model requires the definition of two residual vectors

$$\mathbf{R} = [\mathbf{R}_u, \mathbf{R}_{\tilde{\epsilon}}] \tag{4.1}$$

related to the equilibrium and the averaging equations.

In the work three types of elements are considered, but the general idea for the coupled problem is the following: the elements are three-dimensional and

are based on a standard 8-nodes or 20-nodes (serendipity) topology. They have to describe the two fundamental unknown fields: displacements and averaged measure. The first field is interpolated with the linear or quadratic shape function whereas the second always uses linear interpolation.

In the following solution algorithm the vector of unknowns including both the displacements and non-local variables is denoted by

$$\mathbf{p} = [u_1, u_2, \ldots, u_m, \bar{\epsilon}_1, \bar{\epsilon}_2, \ldots, \bar{\epsilon}_8], \tag{4.2}$$

where m is the number of unknown nodal displacement components for considered element (24 or 60).

5. Solution algorithm

In this section, the AceGen solution algorithm for the elastic-plastic model coupled with gradient-enhanced damage is described.

We consider a time interval $[t_n, t_{n+1}]$ and we know the solution at t_n, particularly, the deformation gradient $\mathbf{F}_n$, the elastic left Cauchy–Green deformation tensor $\mathbf{b}^e_n$, the measure of accumulated plastic flow γ_n and the value of the damage history parameter κ_n. The nodal displacements and the non-local averaged measure $\bar{\epsilon}$ are prescribed at time t_{n+1}. Thus, from a computational point of view, the nonlinear material behaviour is treated as configuration-driven [7]. For the sake of brevity, all quantities related to the current time step t_{n+1} are written without indices.

As it was mentioned, damage and plasticity in the model are indirectly coupled; thus, the code at the level of the individual Gauss point can be divided into three parts including the implementation of:

- the plasticity problem in the effective stress space;
- the damage state in the real stress space;
- the residual vector including the equilibrium and averaging equations, and the consistent tangent matrix.

Consequently, firstly the trial stress state is determined to verify if the plastic regime is entered. Following [9] the relative deformation gradient is computed

$$\mathbf{f} = \mathbf{F}\mathbf{F}_n^{-1}, \tag{5.1}$$

where $\mathbf{F}_n$ is taken from the history and the current value of the deformation gradient is calculated on a basis of interpolated current displacements function $\mathbf{F} = \mathbf{I} + \frac{\partial \mathbf{u}}{\partial \mathbf{X}}$.

Assuming that the relative deformation gradient is elastic the trial elastic left Cauchy–Green tensor is calculated

$$\mathbf{b}^{eT}_{tr} = \mathbf{f}\mathbf{b}^e_n\mathbf{f}^T \tag{5.2}$$

and the corresponding effective trial Kirchhoff stress tensor is derived from the hyperelastic constitutive relation (2.4). Now the yield function (2.13) is computed using the trial Kirchhoff stress tensor and the value of the accumulated plastic strain measure from the previous time step. If the yield function has a negative value then the step is indeed elastic: trial values are the solution in the effective space and the damage should be resolved now. If, on the other hand, the yield criterion is not satisfied, the solution of nonlinear equations including the return map equations and the yield function must be solved [7]

$$\begin{cases} \mathbf{R}_{be} = \mathbf{b}^e - \exp[-2(\gamma - \gamma_n)\mathbf{N}(\hat{\boldsymbol{\tau}}(\mathbf{b}^e))]\mathbf{b}^e_{tr} = 0, \\ R_y = F_p(\hat{\boldsymbol{\tau}}(\mathbf{b}^e), \gamma) = 0. \end{cases} \tag{5.3}$$

The system (5.3) consists of seven scalar equations (due to the symmetry of $\mathbf{b}^e$), with seven unknowns: six components of $\mathbf{b}^e$ and γ. To find a solution of system (5.3) the Newton–Raphson procedure is applied. It should be also added here that in the numerical procedure not the values of components of the elastic left Cauchy–Green tensor $\mathbf{b}^e$ are computed but components of auxiliary tensor $\mathbf{b}^{e*}$, which fulfill the relation $\mathbf{b}^e = \mathbf{f}\mathbf{b}^{e*}\mathbf{f}^T$. The reason for this manipulation is to obtain not only the values of the current tensor $\mathbf{b}^e$ components, but also the functional dependence between the displacements and the deformation tensor $\mathbf{b}^e$, which can be otherwise lost in the iterative procedure of Newton–Raphson.

Now, when the plastic problem is solved and the tensor $\mathbf{b}^e$ is determined, the next step is the verification of the damage condition (2.11a) which takes into account the non-local deformation measure. If the averaged measure exceeds the previous value of the damage history parameter κ_n, then damage increases in relation to the previous time step, and a new value of the history parameter is equal to $\kappa = \bar{\epsilon}$. Otherwise, there is no damage growth and the history parameter does not change its value. The damage variable is computed from Eq. (2.7) using the current value of the history parameter κ and is used for the calculation of degraded free energy function (2.6).

For the uniformity of the residual vector derivation, the potential Π for the averaging differential equation (3.1) is applied in the algorithm. The potential is assumed in such a form that equation $\delta\Pi = 0$ is equivalent to the weak form of Eq. (3.1)

$$\Pi(\bar{\epsilon}, \tilde{\epsilon}) = \frac{1}{2}[(\bar{\epsilon} - \tilde{\epsilon})^2 + l^2 \nabla\bar{\epsilon} \cdot \nabla\bar{\epsilon}], \tag{5.4}$$

where the local deformation measure $\tilde{\epsilon}$ is calculated from (2.9) or (2.10).

Depending on the selected configuration for material or spatial averaging, the potential (5.4) can be expressed in two ways:

$$\Pi_{mat}(\bar{\epsilon},\tilde{\epsilon}) = \frac{1}{2}\left[(\bar{\epsilon}-\tilde{\epsilon})^2 + l_{mat}^2 \frac{\partial\bar{\epsilon}}{\partial\mathbf{X}}\cdot\frac{\partial\bar{\epsilon}}{\partial\mathbf{X}}\right], \tag{5.5}$$

$$\Pi_{spat}(\bar{\epsilon},\tilde{\epsilon}) = \frac{1}{2}\left[(\bar{\epsilon}-\tilde{\epsilon})^2 + l_{spat}^2 \frac{\partial\bar{\epsilon}}{\partial\mathbf{x}}\cdot\frac{\partial\bar{\epsilon}}{\partial\mathbf{x}}\right], \tag{5.6}$$

where $\mathbf{X}$ and $\mathbf{x}$ indicate respectively the Lagrangian and Eulerian coordinates whereas l_{mat} and l_{spat} are internal length parameters specified for initial and current configurations. The relation between the parameters can be derived from the assumption that $\Pi_{mat} = \Pi_{spat}$ which leads to the formula

$$l_{spat} = l_{mat}\sqrt{\frac{\frac{\partial\bar{\epsilon}}{\partial\mathbf{X}}\cdot\frac{\partial\bar{\epsilon}}{\partial\mathbf{X}}}{\frac{\partial\bar{\epsilon}}{\partial\mathbf{x}}\cdot\frac{\partial\bar{\epsilon}}{\partial\mathbf{x}}}}. \tag{5.7}$$

The contribution to the residual vector for elements described in Section 4 can now be defined in the following form

$$\mathbf{R} = \left[\frac{\partial(\psi - W^{ext})}{\partial u_1}, \frac{\partial(\psi - W^{ext})}{\partial u_2}, \ldots, \frac{\partial(\psi - W^{ext})}{\partial u_m}, \frac{\partial\Pi}{\partial\bar{\epsilon}_1}, \frac{\partial\Pi}{\partial\bar{\epsilon}_2}, \ldots, \frac{\partial\Pi}{\partial\bar{\epsilon}_8}\right], \tag{5.8}$$

where W^{ext} is work of the external loads.

Finally, the contribution to the consistent tangent matrix is derived with the formula

$$\mathbf{K} = \frac{\partial\mathbf{R}}{\partial\mathbf{p}}. \tag{5.9}$$

To avoid the differentiation of all steps of the inner Newton–Raphson iterative procedure, the definition of the automatic differentiation exception should be performed to prescribe the derivatives of the internal variables with respect to the independent solution vector. The detailed explanation of the definition of exceptions in differentiation especially for elastic-plastic models is included in [6] and [12].

As it was mentioned, the solution of the described model is obtained using finite elements with first- or second-order interpolation. For the first kind of elements the phenomenon of locking can be observed in plasticity which manifests itself in the spurious hardening in numerical simulations. Apart from the increase of the interpolation order, there are a few methods to prevent standard elements from locking such as the enhanced assumed strain [13], the selective integration or B-bar method [14]. In this work the *F-bar* approach of DE SOUZA NETO *et. al.* is applied [15]. The method involves the replacement of the deformation gradient $\mathbf{F}$ with its modified counterpart $\bar{\mathbf{F}}$. The formulation is based on a multiplicative split of the deformation gradient into its volumetric and isochoric parts

$$\mathbf{F} = \mathbf{F}_{iso}\mathbf{F}_{vol}. \tag{5.10}$$

To calculate $\bar{\mathbf{F}}$ for a Gauss point the volumetric part of the deformation gradient is taken from the centroid of the element whereas the isochoric part is calculated at the proper integration point. The modified deformation gradient is used for all computations and is saved in the history data to be used in the next time step.

The summarized algorithm for the elastic-plastic-gradient-damage material model is presented in Box 1.

Given at element level:

- Isoparametric interpolation.
- Current vector of nodal displacements and non-local variables: $\mathbf{p} = [u_1, u_2, u_3, \ldots, u_{24}, \bar{\epsilon}_1, \bar{\epsilon}_2, \ldots, \bar{\epsilon}_8]$.
- Integration point variables at the end of previous step, i.e., deformation gradient $\mathbf{F}_n$, elastic left Cauchy-Green tensor $\mathbf{b}^e_n$, accumulated plastic flow measure γ_n, and damage history parameter κ_n.

Find at element level:

- Contribution to residual vector and tangent matrix for final values of $\mathbf{b}^e$, γ and κ.

Compute at each integration point:

- Current deformation gradient at given integration point $\mathbf{F} = \mathbf{I} + \frac{\partial \mathbf{u}}{\partial \mathbf{X}}$.
- *For element with F-bar modification:*
  - Current deformation gradient at centroid of element $\mathbf{F}_0$.
  - Modified deformation gradient [15]: $\bar{\mathbf{F}} = \sqrt[3]{\frac{\det(\mathbf{F})}{\det(\mathbf{F}_0)}}\mathbf{F}$.
  - Replacement of deformation gradient $\mathbf{F}$ by $\bar{\mathbf{F}}$.
- Relative deformation gradient: $\mathbf{f} = \mathbf{F}\mathbf{F}_n^{-1}$.
- Trial elastic left Cauchy–Green tensor: $\mathbf{b}^e_{tr} = \mathbf{f}\mathbf{b}^e_n\mathbf{f}^T$.
- Strain potential: $\psi^e(\mathbf{b}^e_{tr})$.
- Trial effective Kirchhoff stress tensor: $\hat{\boldsymbol{\tau}}_{tr} = 2\frac{\partial \psi^e}{\partial \mathbf{b}^e_{tr}}\mathbf{b}^e_{tr}$.
- Yield function for trial effective stress: $F_p(\hat{\boldsymbol{\tau}}_{tr}, \gamma_n)$.
- Yield condition:
  If $F_p < 0$: state is admissible $\rightarrow \mathbf{b}^e = \mathbf{b}^e_{tr}$, $\gamma = \gamma_n$.
  Else, state is inadmissible $\rightarrow \mathbf{b}^e$ and γ computed from:
  $$\begin{cases} \mathbf{R}_{be} = \mathbf{b}^e - \exp[-2(\gamma - \gamma_n)\mathbf{N}(\hat{\boldsymbol{\tau}}(\mathbf{b}^e))]\mathbf{b}^e_{tr} = 0, \\ R_y = F_p(\hat{\boldsymbol{\tau}}(\mathbf{b}^e), \gamma) = 0. \end{cases}$$
- Damage loading function: $F_d(\bar{\epsilon}, \kappa)$.
- Damage condition:
  If $F_d < 0$ then there is no damage growth $\rightarrow \kappa = \kappa_n$.
  Else if $F_d > 0$ then damage grows $\rightarrow \kappa = \bar{\epsilon}$.
- Damage variable: $\omega(\kappa) = 1 - \frac{\kappa_0}{\kappa}\left(1 - \alpha + \alpha \exp(-\beta(\kappa - \kappa_0)\right)$.
- Free energy: $\psi(\mathbf{b}^e, \omega, \gamma) = (1 - \omega)\psi^e(\mathbf{b}^e) + \psi_p(\gamma)$.
- Local strain measure, e.g.: $\tilde{\epsilon} = \det(\mathbf{F}) - 1$.
- Potential for averaging equation: $\Pi(\bar{\epsilon}, \tilde{\epsilon}) = \frac{1}{2}\left((\bar{\epsilon} - \tilde{\epsilon})^2 + l^2 \nabla\bar{\epsilon} \cdot \nabla\bar{\epsilon}\right)$.
- Contribution to residual vector and tangent matrix:
  $\mathbf{R} = \left[\frac{\partial(\psi - W^{ext})}{\partial u_1}, \frac{\partial(\psi - W^{ext})}{\partial u_2}, \ldots, \frac{\partial(\psi - W^{ext})}{\partial u_{24}}, \frac{\partial \Pi}{\partial \bar{\epsilon}_1}, \frac{\partial \Pi}{\partial \bar{\epsilon}_2}, \ldots, \frac{\partial \Pi}{\partial \bar{\epsilon}_8}\right]$, $\quad \mathbf{K} = \frac{\partial \mathbf{R}}{\partial \boldsymbol{p}}$.

Box 1. Finite element algorithm for large strain elasto-plasticity coupled with gradient damage (standard 8-nodes element).

6. Results of numerical simulations

In order to assess the performance of the material model described above, the selected results of numerical simulations are presented. All tests have been performed using finite element environment AceFEM [6]. Due to the complexity of the examined model selected aspects have been analysed. Firstly, test results related to different finite element types are presented, secondly a comparison of spatial and material averaging for the hyperelastic-gradient-damage model is performed and finally simulations for the different non-local strain measures are included.

In the following simulations two specimens are analysed: a bar with variable cross-section along the length (VCSB) and a perforated plate (PP) – both specimens are in tension. The dimensions and the boundary conditions of the samples are presented in Figs. 1 and 3, whereas the applied discretizations in Figs. 2 and 4.

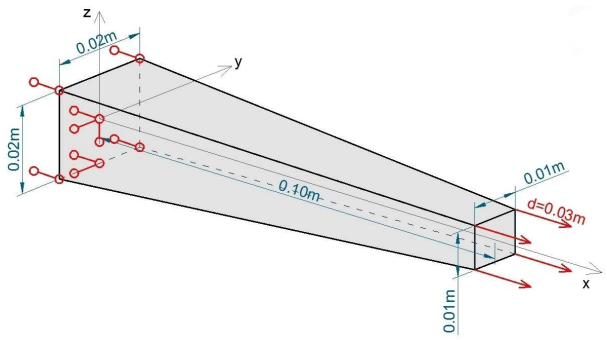

FIG. 1. Geometry and boundary conditions for VCSB.

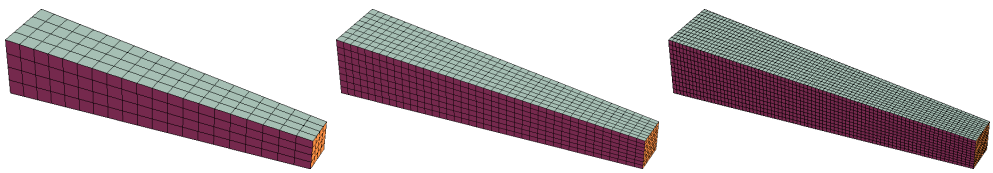

FIG. 2. Discretizations of VCSB: $20 \times 4 \times 4$ (coarse mesh), $40 \times 8 \times 8$ (medium mesh) and $80 \times 12 \times 12$ (fine mesh).

The statement of the material laws and parameters which are applied in the simulations are presented in Tables 1 and 2. If other formulas or values are considered then it is stated in the test description.

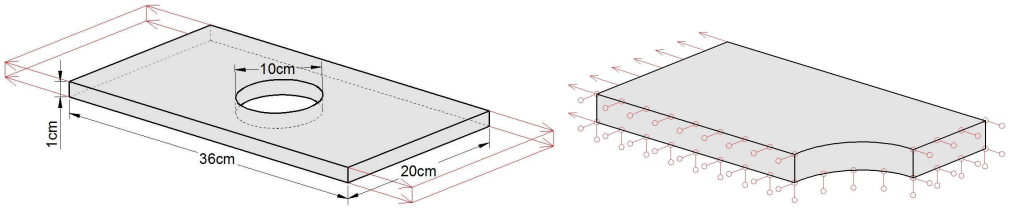

Fig. 3. Geometry and boundary conditions for PP.

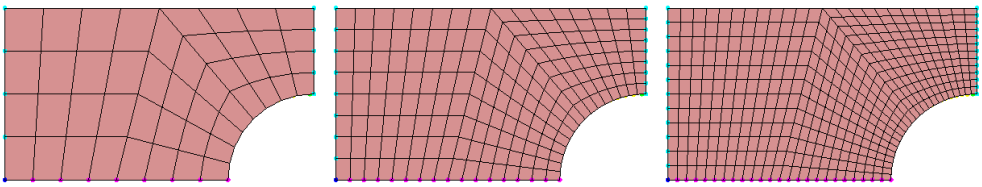

Fig. 4. Discretizations of PP: 48, 192 and 432 elements.

Table 1. Summary of material laws used for numerical simulations.

Description	Formula
Elastic free energy [9]	$\psi^e(\mathbf{b}^e) = 0.5K[0.5(\det(\mathbf{b}^e) - 1) - 0.5\ln(\det(\mathbf{b}^e))]$ $+0.5G(\mathrm{tr}(\det(\mathbf{b}^e)^{-1/3}\mathbf{b}^e) - 3)$
Damage evolution law [16]	$\omega(\kappa) = 1 - (\kappa_0/\kappa)\,(1 - \alpha + \alpha\exp(-\beta(\kappa - \kappa_0))$
Measure governing damage	$\epsilon = \det(\mathbf{F}) - 1$
Plasticity function	$f(\hat{\boldsymbol{\tau}}) = \sqrt{2J_2} + (\alpha_p/3)I$

Table 2. Summary of material properties used for numerical simulations.

Property	Symbol	Value	Unit
Young modulus	E	200e9	Pa
Poisson ratio	ν	0.3	–
Damage threshold	κ_0	0.04	–
Damage evolution law parameter	α_d	0.95	–
Damage evolution law parameter	β_d	5	–
Internal length scale for material averaging	l_{mat}	0.01	m
Internal length scale for spatial averaging	l_{spat}	0.01	m
Initial compression yield threshold	σ_{c0}	1.225e9	Pa
Initial tension yield threshold	σ_{t0}	1.225e9	Pa
Hardening modulus	h	20e9	Pa

6.1. Tests for different elements

The first group of simulations is performed for different types of the finite elements. Particularly, the following ones are taken into account:

- elements H1 – standard eight-noded hexahedron with linear interpolation of the displacement and non-local variable fields,
- elements H1+$\bar{\mathbf{F}}$ – eight-noded hexahedron with linear interpolation of the unknown fields and the *F-bar* approach applied,
- elements H2S – standard 20-noded Serendipity hexahedron with quadratic interpolation of displacements and linear interpolation of the non-local variable field.

The first simulation is performed for the material model of hyperelasticity-plasticity and the VCSB specimen. The diagram presenting the sum of reactions on the supported end of the sample versus the displacement imposed at the other end is shown in Fig. 5. It can be observed that the curves for elements H1 differ significantly from the other curves and they depend on the adopted discretization. The reason for that behaviour is the locking phenomenon which causes a stiffer sample response. The results for elements H1 + $\bar{\mathbf{F}}$ and elements H2S coincide in the pre-peak regime. For each diagram, softening of the material can be observed which is caused by the geometrical effects – necking. This phenomenon occurs although plasticity with hardening is applied. In the post-peak regime the results differ for each mesh which motivates regularization.

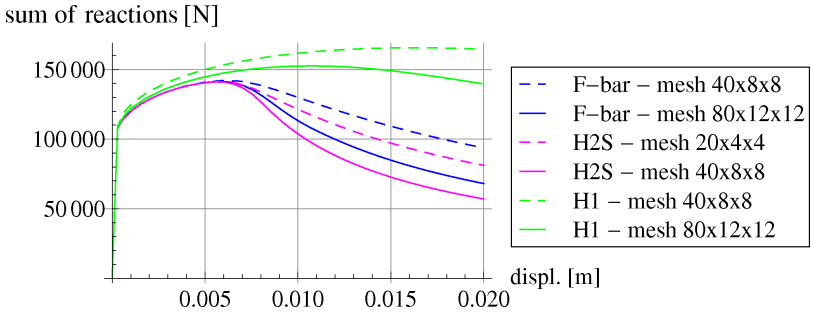

FIG. 5. Sum of reactions vs displacements for different elements (hyperelasticity-plasticity, VCSB).

The second test is performed using PP and hyperelastic-plastic model coupled with gradient damage. In this test the damage threshold is assumed to be equal to $\kappa_0 = 0.003$ and material averaging is applied with internal length $l_{mat} = 0.02$.

The graph presenting the sum of reactions vs enforced displacement is presented in Fig. 6. It can be noticed that the behaviour of the hyperelastic-plastic material (dashed lines) is similar to the previous test: the results for elements H1 + $\bar{\mathbf{F}}$ and H2S are similar whereas the model simulated with elements H1 ex-

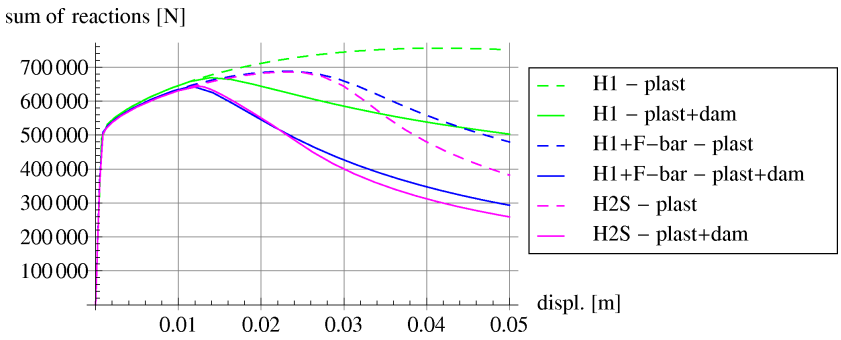

Fig. 6. Sum of reactions vs stretch ratio (hyperelasticity-gradient-damage-plasticity, PP).

hibits a larger stiffness. Also in this test, in spite of plasticity with hardening, necking can be observed. If the model coupled with gradient damage is taken into account, then the results for H1$+\bar{\mathbf{F}}$ and H2S coincide up to beginning of the necking process (for $u \approx 0.024$ m). It can be noticed that although the gradient averaging is applied in the model it does not preserve the numerical results from the mesh-sensitivity for the softening caused by geometrical effects.

Taking the observation from these simulations into account the following computations are performed for elements H1 $+ \bar{\mathbf{F}}$.

6.2. Spatial vs material averaging

As it was mentioned, gradient averaging applied to large strains can be performed in the undeformed or in the current configuration. To investigate the behaviour of models with these two kinds of averaging methods the following numerical tests are performed.

Firstly, the VCSB example is analysed. The application of the sample whose cross-section is variable along the length causes that the cross-section where damage occurs at first is prescribed – it is the narrowest end of the bar. The internal length parameter is assumed to be constant $l = 0.01$ during deformation process and has the same value for both material and spatial averaging. This group of tests is performed for the hyperelasticity-gradient-damage model.

Figure 7 depicts the sum of reactions for the enforced displacements.

Although the simulations are performed with identical material parameters, the response for the two types of averaging differs significantly. Firstly, it can be observed that the post-peak branch for the model with spatial averaging descends more rapidly than for material averaging. Secondly, the application of spatial averaging does not result in mesh-insensitivity: for each discretization the diagram is different. The results for material averaging for all analysed discretizations are close, and the diagrams for the second and the third mesh almost coincide.

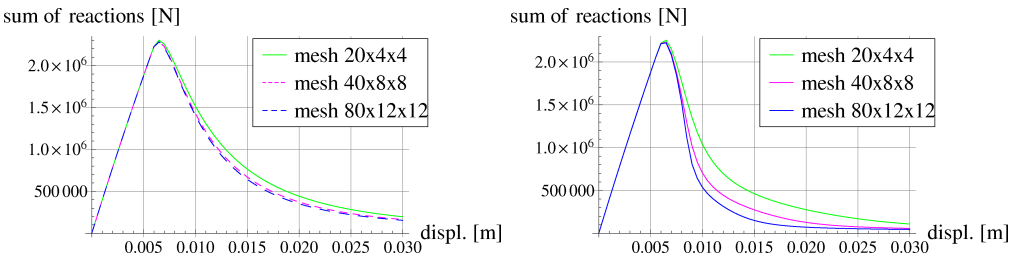

FIG. 7. Displacement vs reaction sum for material and spatial averaging and different discretizations.

It is shown in Figs. 8 and 10 how the specimen deforms and how the first component of the Green strain tensor E_{xx} and damage variable ω are distributed. Moreover, in Fig. 9 the evolution of E_{xx} along the bar length is depicted.

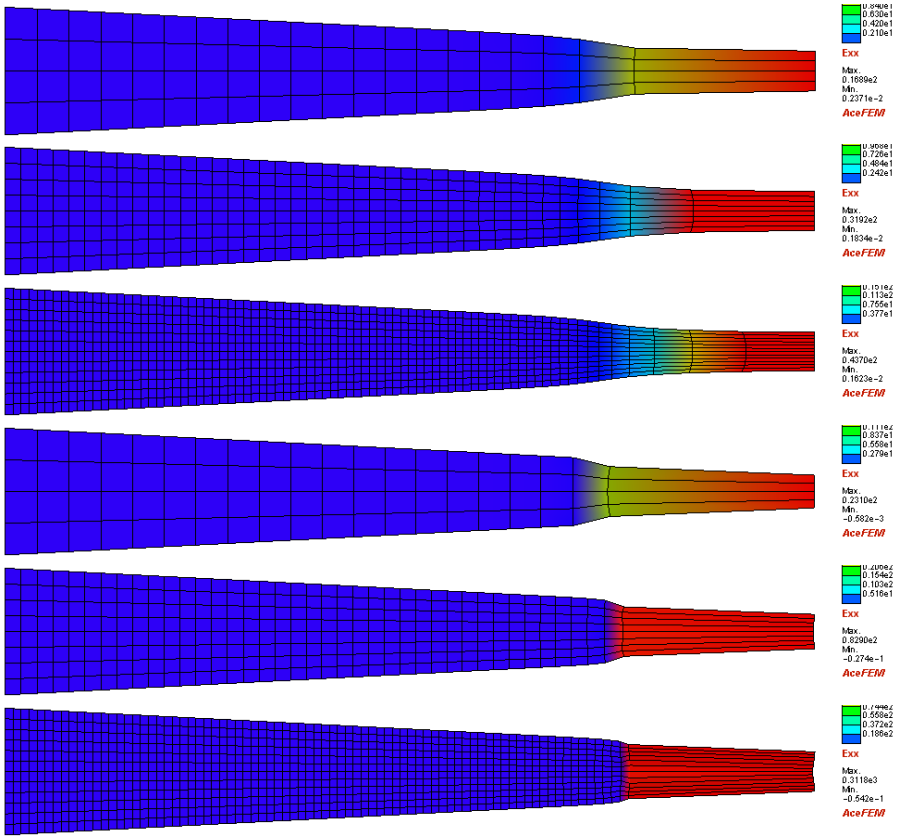

FIG. 8. Deformed meshes at the end of tension test with E_{xx} distribution for material averaging (upper three pictures) and spatial averaging (lower three pictures) – hyperelasticity-gradient-damage, VCSB.

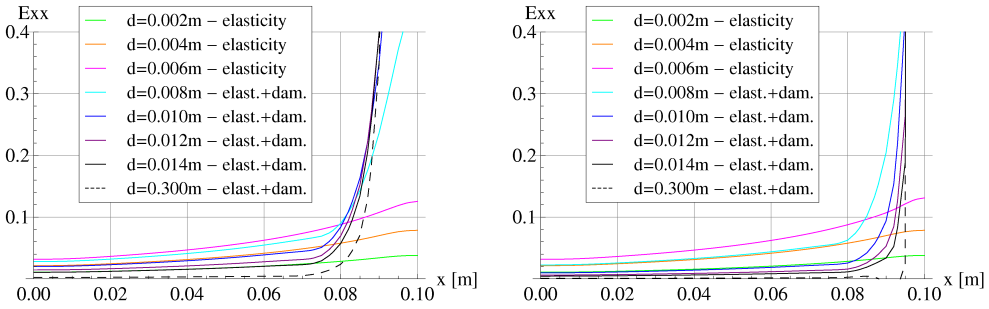

Fig. 9. Evolution of the first component of Green strain tensor E_{xx} for material (on the left) and spatial (on the right) averaging – medium mesh (hyperelasticity-gradient-damage, VCSB).

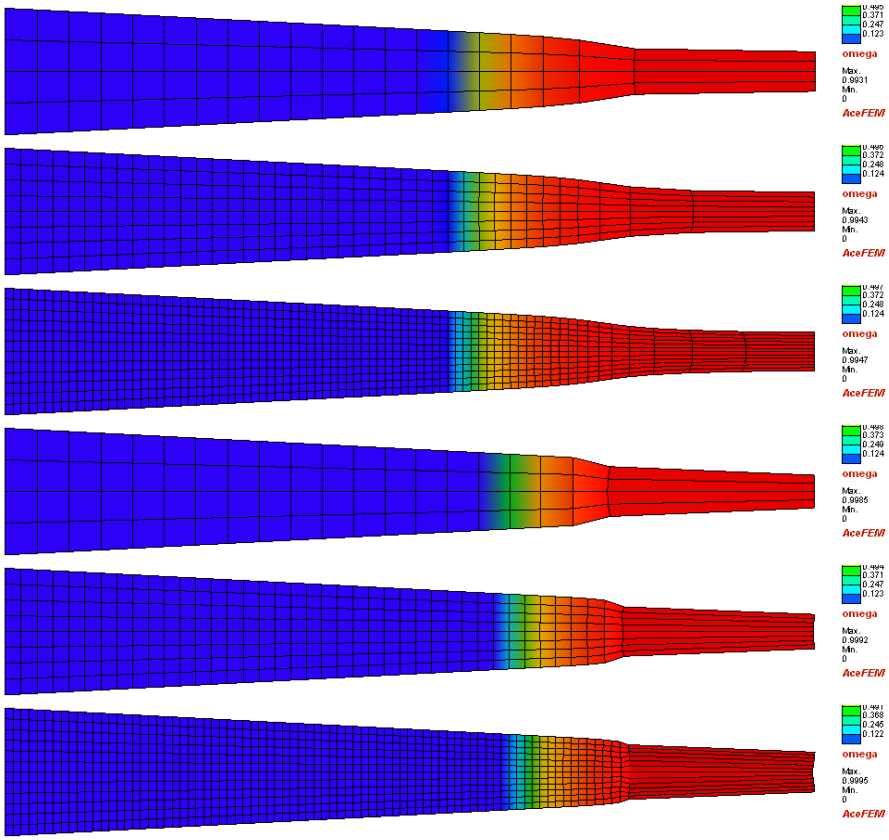

Fig. 10. Deformed meshes at the end of tension test with damage variable ω distribution for material averaging (upper three pictures) and spatial averaging (lower three pictures).

It can be observed that for spatial averaging the deformation and the strain distribution depend on the finite element discretization, whereas for material averaging the response is similar for different meshes. It can be noticed in Fig. 9 that as the enforced displacement increases the strain localization zone gets narrower for spatial averaging. For large enough deformation, strains concentrate in one row of elements for all analysed discretizations. Although in the considered description the gradient regularization is applied, it does not fully preserve the numerical simulations from the pathological mesh-sensitivity.

It can be noticed in Fig. 10 that the damage zone is similar for all discretizations for spatial averaging although the deformation differs significantly. The phenomenon is caused by irreversibility of the state of material damage. The damage area which arises at the beginning of the loading process does not become smaller even if deformations concentrate in the gradually smaller band and the rest of the sample is unloaded.

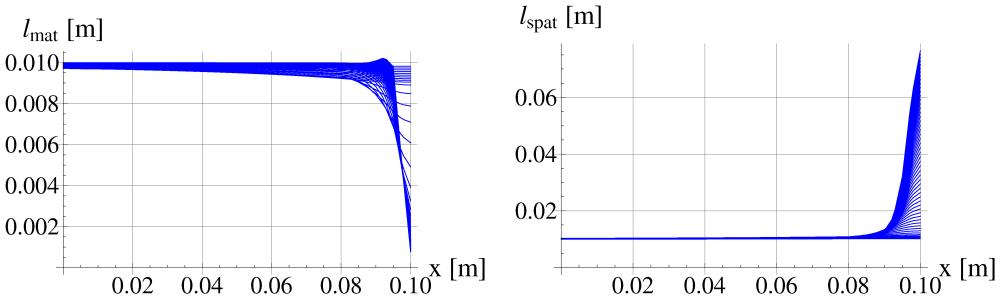

FIG. 11. Evolution of material internal length whereas spatial is fixed and conversely, mesh $40 \times 8 \times 8$.

The phenomenon of mesh-sensitivity observed for spatial averaging was noticed by STEINMANN [3], however without detailed explanation. To investigate the reason for such a behaviour, the evolution of material or spatial length scale parameters for the two kinds of averaging are studied (Fig. 11). The relation between parameters presented in Fig. 11 is expressed through Eq. (5.7). In the first diagram we can observe the evolution of the material internal length along the bar for the medium mesh whereas the spatial one is fixed. The value of the length parameter decreases in the damage zone with increasing loading. On the other hand, if the material internal length is fixed, the value of the spatial one grows at the end of the bar with the smaller cross-sectional area. It can also be observed that for spatial averaging the corresponding material length scale at the narrowest end of the bar decreases to the value less than 0.001 m whereas the size of element for the medium mesh is equal to 0.0025 m. Numerical experiments reveal that for the assumed material parameters and the VCSB specimen (mesh

$40 \times 8 \times 8$) the application of the constant internal length for material averaging less than 0.002 m results in the localization of strains in one row of elements.

For the deformation process performed for spatial averaging it can be observed that the zone where the strains grow gradually narrows and finally reduces to one row of elements when the corresponding material, internal length is small enough.

To conclude, the averaging performed with the constant spatial internal scale and fixed mesh in the deformed configuration causes the effect that for strains large enough the gradient enhancement does not preserve the solution from the mesh sensitivity. For spatial averaging an adaptative mesh refinement can be considered to remove the dependency on the discretization.

6.3. Tests for different strain measures

In the following simulations the dependence of the results on the adopted strain measure which governs the damage evolution is investigated. Two measures introduced in Section 2 are taken into account:

$$\tilde{\epsilon}_1 = \det(\boldsymbol{F}) - 1, \qquad \tilde{\epsilon}_2 = \sqrt{(e_1^+)^2 + (e_2^+)^2 + (e_3^+)^2}.$$

Firstly, the simulations for VCSB are performed for the coarse and the medium mesh, and the hyperelastic-damage model with material averaging. In order to initiate the damage process at the same moment in the two considered cases, the damage threshold is assumed different for each measure: $\kappa_{0,\tilde{\epsilon}_1} = 0.04$ and $\kappa_{0,\tilde{\epsilon}_2} = 0.085$.

In Fig. 12 the sum of reactions vs enforced displacements diagram is depicted. It can be observed that the results significantly differ for the two measures. If we assume the same damage evolution law with identical material parameters (as in Tables 1 and 2), then the model with $\tilde{\epsilon}_1$ exhibits much lower stiffness whereas for $\tilde{\epsilon}_2$ the sum of reactions is degraded to a lesser extent. To verify if the

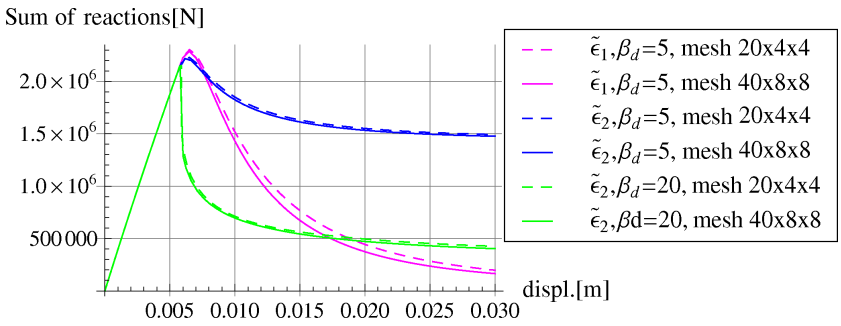

Fig. 12. Sum of reactions for hyperelasticity-gradient-damage model with different deformation measures – VCSB.

difference is a result of the adopted parameters of the damage evolution law, the tests for $\tilde{\epsilon}_2$ and the higher value of parameter $\beta_d = 20$ are performed. It turns out that although the sum of reactions reaches values smaller than previously, the diagram behaves in a different way: the loss of stiffness is very rapid in the first phase of the damage process and later it is more gentle, whereas for $\tilde{\epsilon}_1$ the diagram descends rather uniformly. In the post-peak regime the snap-back would probably be observed if the arc-length control was applied instead of the enforcing displacement.

When analysing the deformed mesh with the non-local variable distribution (Fig. 13), the difference in the sample shape at the end of the deformation process can be noticed. For each test the deformation of the finite element mesh is different. Moreover, for $\tilde{\epsilon}_1$ the non-local variable is almost twice larger than for $\tilde{\epsilon}_2$.

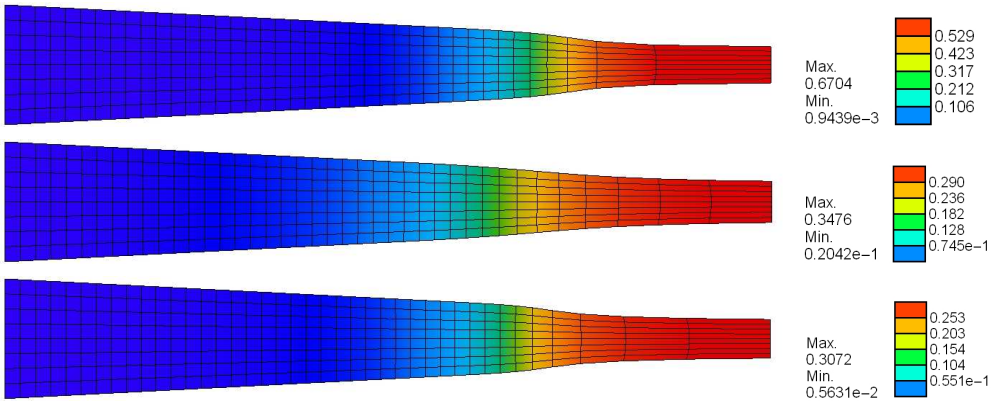

FIG. 13. Deformed mesh and non-local variable distribution for: 1) $\tilde{\epsilon}_1$ and $\beta_d = 5$, 2) $\tilde{\epsilon}_2$ and $\beta_d = 5$, 3) $\tilde{\epsilon}_2$ and $\beta_d = 20$.

The second test is performed for the PP specimen with the same material parameters as previously apart from the internal length which is assumed to be $l = 0.02$ m. The sum of reactions vs displacement diagram (Fig. 14) is similar to the response of VCSB: for the different measures governing damage the diagram presents the various responses of the sample.

On the other hand, if the material model including plasticity coupled with gradient damage is considered (Fig. 15), then the sum of reactions diagrams for the models with different strain measures are very close (notice however that we assumed $\kappa_{0,\tilde{\epsilon_1}} = 0.003$ and $\kappa_{0,\tilde{\epsilon_2}} = 0.007$).

Taking into account these results, we conclude that the strain measure applied to the model is of high significance for hyperelasticity with damage and should be carefully selected for a specific material to be analysed. For the material model coupled with plasticity the choice of $\tilde{\epsilon}$ does not influence the results strongly.

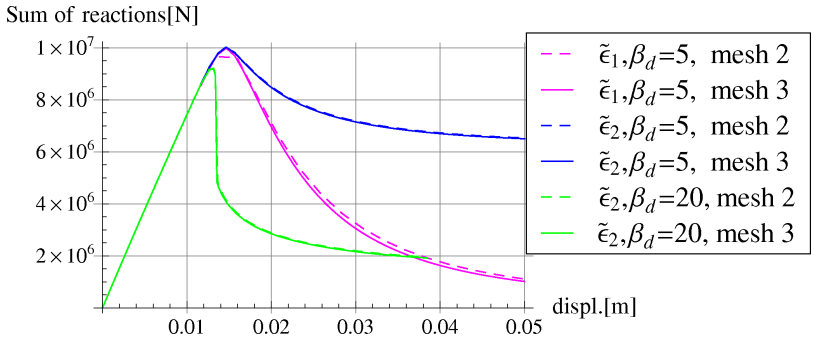

Fig. 14. Sum of reactions for hyperelasticity with gradient damage with different deformation measures – PP.

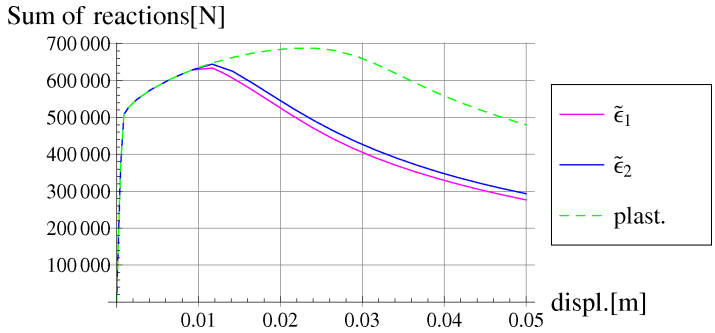

Fig. 15. Sum of reactions for hyperelasticity-gradient-damage-plasticity model with different deformation measures – PP.

7. Conclusion

In this paper, the framework of the gradient-enhanced large-strain elasticity-damage-plasticity model has been outlined. The model is based on the multiplicative decomposition of the deformation gradient (2.1), the Helmholtz free energy in the form (2.3) and is limited to isotropy and isothermal conditions. The gradient averaging is applied to the deformation measure which determines the damage growth. The selected aspects of the implementation within AceGen package are discussed and the detailed presentation of solution algorithm is included. The application of the advanced symbolic computation tool gives the authors the possibility to focus on the analytical model instead on FEM programming.

The selected results of the computational tests for the analysed model have been presented. Firstly, the influence of the adopted finite element types has been investigated. The presented numerical results show that the standard eight-noded hexahedral elements cannot properly reproduce plasticity due to the phe-

nomenon of volumetric locking. The problem can be solved using the elements with a higher-order approximation or by a proper modification of the standard elements, for example the *F-bar* approach. Both possibilities have been considered in the work and it turns out that both are able to simulate a plastic process successfully. Therefore, and because of a smaller cost of computations, the standard elements with the *F-bar* amendment are employed in further computations.

Since a comprehensive analysis of the configuration selection for gradient averaging seems to be missing in the literature (apart from the publication of Steinmann [3]), this issue has been examined in the paper. The numerical results reveal that the averaging performed in the current configuration does not fully prevent the results from the pathological mesh sensitivity as opposed to material averaging. This situation is caused by the change of element size during localization whereas the internal length parameter is assumed to have a constant value in the current configuration during whole deformation process.

The problem of the choice of a deformation measure governing damage has also been analysed. Two different measures have been taken into account and tested using different specimens. It turns out that the selection of the deformation measure can strongly influence the results for the hyper-elastic model coupled with gradient averaging. Consequently, the application of a proper measure which can correctly reproduce the behaviour of a real material is an important aspect of constitutive modeling.

Moreover, it should be stressed that neglecting the assumption of small deformation induces also the geometrical effect of necking which causes mesh-sensitivity in the simulations even though the gradient averaging is applied in the model. The proper reproduction of geometrical softening observed for plasticity should be further investigated. Moreover, an adaptive mesh refinement is especially advisable for the spatial averaging. The research is also planned to be extended towards thermo-mechanical coupling.

Acknowledgments

The authors acknowledge fruitful discussions on the research with Prof. S. Stupkiewicz from IPPT, Warsaw, Poland.

The research has been carried out within the grant from Doctus-Małopolska doctoral scholarship fund.

The contribution of the second author was supported by the European Union through the European Social Fund within project "Cracow University of Technology development program – top quality teaching for the prospective Polish engineers; University of the 21st century" (contract no.UDA-POKL.04.01.01-00-029/10-00).

References

1. H. Li, N. Chandra, *Analysis of crack growth and crack tip plasticity in ductile materials using cohesive zone models*, Int. J. Plasticity, **19**, 849–882, 2003.
2. R.H.J. Peerlings, R. de Borst, W.A.M. Brekelmans, J.H.P. de Vree, *Gradient-enhanced damage for quasi-brittle materials*, Int. J. Numer. Meth. Engng., **39**, 3391–3403, 1996.
3. P. Steinmann, *Formulation and computation of geometrically non-linear gradient damage*, Int. J. Numer. Meth. Engng., **46**, 5, 757–779, 1999.
4. M.G.D. Geers, *Finite strain logarithmic hyperelasto-plasticity with softening: a strongly non-local implicit gradient framework*, Comput. Methods Appl. Mech. Engrg., **193**, 3377–3401, 2004.
5. P.M.A. Areias, J.M.A. César de Sá, C.A. Conceição, *A gradient model for finite strain elastoplasticity coupled with damage*, Finite Elements in Analysis and Design, **39**, 13, 1191–1235, 2003.
6. J. Korelc, *Automation of primal and sensitivity analysis of transient coupled problems*, Computational Mechanics, **44**, 631–649, 2009.
7. F. Auricchio, R. L. Taylor, *A return-map algorithm for general associative isotropic elasto-plastic materials in large deformation regimes*, Int. J. Plasticity, **15**, 1359–1378, 1999.
8. T. Żebro, K. Kowalczyk-Gajewska, J. Pamin, *A geometrically nonlinear model of scalar damage coupled to plasticity* Technical Transactions, **20**, 251–262, 2008; Series Environmental Enginnering 3-Ś/2008.
9. J.C. Simo, T.J.R. Hughes, *Computational Inelasticity. Interdisciplinary Applied Mathematics, Vol. 7*, Springer, New York, 1998.
10. J. Lemaitre, *Coupled elasto-plasticity and damage constitutive equations*, Comput. Methods Appl. Mech. Engrg., **51**, 31–49, 1984.
11. T. Belytschko, D. Lasry, *A study of localization limiters for strain-softening in statics and dynamics*, Comput. & Struct., **33**, 707–715, 1989.
12. P. Wriggers, *Nonlinear Finite Element Methods*, Springer, Berlin, Heidelberg, 2008.
13. J.C. Simo, M.S. Rifai, *A class of mixed assumed strain methods and the method of incompatible modes*, Int. J. Numer. Meth. Engng., **29**, 1595–1638, 1990.
14. T.J.R. Hughes, *Generalization of selective integration procedures to anisotropic and nonlinear media*, Int. J. Numer. Meth. Engng., **15**, 1413–1418, 1980.
15. E.A. de Souza Neto, D. Peric, D.R.J. Owen, *Computational Methods for Plasticity. Theory and Applications*, John Wiley & Sons, Ltd, Chichester, UK, 2008.
16. J. Mazars, G. Pijaudier-Cabot, *Continuum damage theory – application to concrete*, ASCE J. Eng. Mech., **115**, 345–365, 1989.

Received December 28, 2012; revised version April 15, 2013.